

DOI: 10.1002/((please add manuscript number))

**Article type: Communication**

### **UV-assisted Low Temperature Oxide Dielectric Films for TFT Applications**

*Jaeun Hwang,<sup>1</sup> Kyungmin Lee,<sup>1</sup> Yesul Jeong,<sup>2</sup> Yong Uk Lee,<sup>3</sup> Christopher Pearson,<sup>2</sup>  
Michael C. Petty,<sup>2</sup> Hongdoo Kim<sup>1\*</sup>*

Jaeun Hwang,<sup>1</sup> Kyungmin Lee,<sup>1</sup> Yesul Jeong,<sup>2</sup> Yong Uk Lee,<sup>3</sup> Christopher Pearson,<sup>2</sup>  
Prof. Michael C. Petty,<sup>2</sup> Prof. Hongdoo Kim<sup>1\*</sup>

<sup>1</sup>Department of Advanced Materials Engineering for Information and Electronics, Kyung Hee University, Yongin 446-701, Korea.

<sup>2</sup>School of Engineering and Computing Sciences and Centre for Molecular and Nanoscale Electronics, Durham University, South Road, Durham DH1 3LE, UK.

<sup>3</sup>Centre for Process Innovation Limited, Thomas Wright Way, Sedgefield, Durham TS21 3FG, UK.

E-Mail: hdkim@khu.ac.kr

Keywords: UV-assisted annealing, gate insulator, oxide dielectrics, metal nitrate, ZnO TFT

Solution-processed metal oxide thin-film transistors (TFTs) have been widely studied for flexible, large-area, printed-electronics applications.<sup>[1-3]</sup> To date, the research effort has focused on improving the semiconductor materials<sup>[4, 5]</sup>, devising **dielectric material formulations with optimized structures**<sup>[6, 7]</sup>, and on using low-temperature processing<sup>[8-11]</sup> in order to achieve compatibility with plastic substrates. Among the various methods investigated, ultraviolet (UV) photochemical activation of sol-gel precursors is particularly significant, as the technique can also be adapted to form the gate insulator.<sup>[10, 11]</sup>

For the successful realization of printed or plastic electronics, high quality dielectrics, deposited via a solution-based process, are also required. In this respect, it should be noted that the development of suitable gate materials has received significantly less attention than the active semiconductor layers. Desirable requirements for gate insulators include large permittivities, low leakage current densities, **an optimized structure with smooth interfaces**<sup>[6, 7]</sup> and also the possibility of low temperature processing.<sup>[12]</sup> The availability of ultra-thin, high-dielectric-constant (high-k) gate insulators will reduce significantly the operating voltage of solution processed oxide TFTs (currently a few tens of volts).<sup>[13]</sup> However, there are few reports of solution-processed gate insulators that fulfill the above requirements and that can be deposited at a sufficiently low temperature.

Of the various inorganic dielectrics studied, the best candidates for low-voltage, solution-processed oxide TFTs are zirconium oxide ( $ZrO_2$ ), hafnium oxide ( $HfO_2$ ), aluminum oxide ( $Al_2O_3$ ), yttrium oxide ( $YO_2$ ) and their mixtures. Such compounds possess high dielectric constants, large conduction band offsets and excellent solvent resistance.<sup>[14-16]</sup> These materials are generally vacuum deposited<sup>[6, 7, 15]</sup> or require relatively high post-annealing temperatures.<sup>[17-20]</sup>

To reduce the processing temperature, Park et al. have utilized an UV-annealing method to prepare ZrO<sub>2</sub> dielectrics from zirconium acetylacetonate.<sup>[21]</sup> Subsequently, Xu et al.,<sup>[22]</sup> Park et al.<sup>[12]</sup> and Lin et al.<sup>[11]</sup> adopted the same method to demonstrate that low-voltage TFTs could be achieved by combining the low-temperature, solution-processed ZrO<sub>2</sub> dielectric layer with either ZnO or an organic semiconducting channel. However, during the conversion from metal acetylacetonate to metal oxide, nano-pores can be generated in the gate insulator layer. These result from the relatively large size of the acetylacetonate moiety, which decomposes into organic vapor during the UV exposure. As a consequence, the gate leakage current densities reported are relatively high, around 10<sup>-6</sup> A/cm<sup>2</sup> at 1 MV/cm.

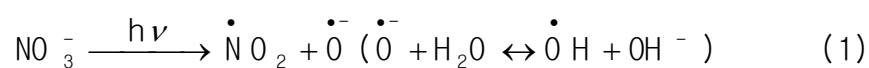
In this work, inorganic nitrate salts were used to form oxide dielectric layers below 150 °C with UV-assisted thermal annealing. The nitrate salts absorb UV light at a wavelength of around 200 nm and, with appropriate thermal energy, readily decomposes into NO<sub>x</sub>. Since the nitrate group is much smaller than acetylacetonate, the resulting oxide dielectric layer will have fewer nano-pores, which should lead to lower leakage currents. **This may be confirmed by thickness changes<sup>[12]</sup> and surface ellipsometric measurements<sup>[23]</sup> during UV-assisted thermal annealing.** Furthermore, inorganic nitrate salts are low-cost and readily available. Here, we present a study of the processing of two nitrate salts to form dielectric oxide layers. The resulting thin films are shown to be excellent electrical insulators, which may be exploited in TFT applications.

## Results and Discussion

As shown in Figure S1, the UV absorption spectra of zirconium oxynitrate and aluminum nitrate in aqueous solutions are identical for the same solution concentrations. This is expected, as the absorption originates from the nitrate ion. The UV absorption spectrum of NO<sub>3</sub><sup>-</sup>(aq) is well understood and consists of two bands. The first (corresponding to the  $\pi^* \leftarrow \pi$

transition) is a highly intensive peak at approximately 200 nm, with an absorption coefficient  $\varepsilon = 9900 \text{ M}^{-1} \text{ cm}^{-1}$ . The other band, centered at 300 nm, is much weaker ( $\varepsilon = 7.2 \text{ M}^{-1} \text{ cm}^{-1}$ ) and is assigned to the  $\pi^* \leftarrow n$  transition.<sup>[24-26]</sup>

The nitrate ion will readily decompose under UV exposure, as described by Equations (1) - (3) below. It has been suggested that excitation in the  $\pi^* \leftarrow \pi$  band ( $\lambda < 280 \text{ nm}$ ) proceeds via the two primary photo processes (1) and (2), whereas excitation in the  $\pi^* \leftarrow n$  band ( $\lambda > 280 \text{ nm}$ ) proceeds through steps (1) and (3).<sup>[27-29]</sup>



Although the UV photo-degradation mechanisms of the nitrate ion are complex, oxygen and nitrogen dioxide radicals are formed during UV exposure and the metal nitrate eventually turns into the metal oxide.

Outside the water environment, the absorption peaks are shifted to lower wavelength. The UV absorption spectra for both metal nitrates coated onto quartz substrates are shown in Figure S2. Data are also included for the effects of pre-heating the films and of their subsequent UV exposure. However, because of the limited range of our UV spectrometer, it is difficult to discern the detailed changes occurring during the heating and irradiation.

The thicknesses of zirconium oxynitrate and aluminum nitrate films were therefore **monitored by a surface profiler** during UV exposure at 150 °C, as shown in **Figure 1**. **Although there is an inaccuracy in measuring the thickness with the surface profiler, it is possible to deduce the general trend of thickness change during UV-thermal annealing for a given sample.** The

thickness of the zirconium oxynitrate film reduced from 55 nm to 31 nm, about 57% of the initial thickness. Assuming that the overall volume change of film occurs in the  $z$ -direction and that the density of the film does not vary during UV annealing, the thickness change will be proportional to the molar mass change, expected to be 53%. This is in broad agreement with the figure of 28% for the thickness change using zirconium acetylacetonate reported by Park et al.,<sup>[12]</sup> which is consistent with the theoretical value (25.3%) noted by this group. Although these workers prepared their ZrO<sub>2</sub> films with UV irradiation (but without thermal annealing) the observed leakage current density is rather large. This behavior may be due to film shrinkage during UV exposure. As noted above, the acetylacetonate group has a large molecular mass compared with the nitrate group, and many voids and defects will probably be generated. In this sense, our metal nitrate system is preferred to the metal acetylacetonate.

To understand further the properties of our dielectric layers, surface ellipsometric measurements were undertaken. Two different models were used to fit the data: 1) a simple model based on varying the thickness and refractive index to deduce the optical constants of the coated material; and 2) use of the Bruggeman EMA (effective medium approximation) model with a reference material and voids in order to estimate the void concentration within the coated layer. The refractive indices of both Al<sub>2</sub>O<sub>3</sub> and ZrO<sub>2</sub> dielectric films were extracted by using the reference material optical constants as an initial guess, as given in Figure 2.

Measured and model-fitted results for  $\Psi$  and  $\Delta$  as well as  $\langle n \rangle$  and  $\langle k \rangle$ , using the WVASE32 program, are provided in Figure S3 and Table 1; both models behave very well judging from root mean square error (MSE). In the case of Al<sub>2</sub>O<sub>3</sub> dielectric layers prepared from Al(OH)<sub>3</sub> and Al(NO<sub>3</sub>)<sub>3</sub> precursor solutions (according to the recipes in Table 2) the void concentrations are estimated to be 33.1% and 25.7%, respectively, using EMA model. Also, as shown in Figure 2, the refractive indices of the Al<sub>2</sub>O<sub>3</sub> film prepared from Al(NO<sub>3</sub>)<sub>3</sub> are higher than those

prepared from  $\text{Al}(\text{OH})_3$ , indicating that the former layer is denser than the latter. In the case of the  $\text{ZrO}_2$  dielectric film, with or without the  $\text{Al}_2\text{O}_3$  bottom layer prepared from  $\text{Al}(\text{OH})_3$  precursor solution, the  $\text{ZrO}_2$  dielectric is fitted well by both models. The refractive indices of our  $\text{ZrO}_2$  film are smaller than those of  $\text{ZrO}_2$  produced by DC magnetron sputtering<sup>[30]</sup>. With the EMA model, the void percentages of  $\text{ZrO}_2$  films with and without  $\text{Al}_2\text{O}_3$  layer are estimated to be 15.5 and 15.4%, respectively. Although the estimated void concentration of the  $\text{ZrO}_2$  layer is lower than that of  $\text{Al}_2\text{O}_3$  film, we cannot conclude that the  $\text{ZrO}_2$  film is denser than the  $\text{Al}_2\text{O}_3$  layer as the estimation of voids depends on the reference material used. Since our  $\text{ZrO}_2$  and  $\text{Al}_2\text{O}_3$  films are very smooth (see Figure 5), the surface roughness of the interface was not included in our model. In fact, including the surface roughness did not improve the fitting quality in the ellipsometry analysis judging from the MSE values. According to XRD data, as given in Figure S4, both the  $\text{Al}_2\text{O}_3$  and  $\text{ZrO}_2$  films possess amorphous structures, even though there is a broad peak for the  $\text{ZrO}_2$  film. The presence of this peak around  $33^\circ$  suggests that some short-range ordering exists in the films, but crystallization does not occur.<sup>[6]</sup>

To examine the detailed compositions of oxide dielectrics, XPS spectra were obtained from both  $\text{ZrO}_2$  and  $\text{Al}_2\text{O}_3$ , shown in Figure 3. Compared to the reference spectra from the literature, both samples reveal a high O1s peak, which may be due to hydroxyl OH radical formation during the UV annealing process, as indicated by Equation (1). In the particular case of  $\text{Al}_2\text{O}_3$ , an hydroxyl gel form may be produced by dangling OH groups in the early stage of annealing. This could prevent further conversion to  $\text{Al}_2\text{O}_3$ , resulting in the slightly smaller percentage thickness change, which may reflect the fact that the  $\text{Al}_2\text{O}_3$  film prepared from  $\text{Al}(\text{OH})_3$  possesses a higher void percentage than the film prepared from  $\text{Al}(\text{NO}_3)_3$  (according to our previous ellipsometry results).

Figure 4 shows SEM images of  $\text{ZrO}_2$  and  $\text{Al}_2\text{O}_3$  films prepared from metal precursor solutions. The thicknesses of both samples depend on the solution concentration. A thick layer can be prepared easily, either by using higher concentrations or by multiple coatings. Below 13 wt %  $\text{ZrO}_2$  precursor solution, the interfaces between each layer in the stack cannot be distinguished. For the  $\text{Al}_2\text{O}_3$  film prepared from either  $\text{Al}(\text{NO}_3)_3$  or  $\text{Al}(\text{OH})_3$ , it is hard to distinguish the interface between Si substrate and  $\text{Al}_2\text{O}_3$ . In this case, the Si substrate with a 300 nm  $\text{SiO}_2$  layer was used to determine the thickness of  $\text{Al}_2\text{O}_3$  dielectric layer. Following the photo-decomposition and densification, AFM studies, Figure 5, indicate that the films have become significantly smoother. For example, the RMS roughnesses of  $\text{ZrO}(\text{NO}_3)_2$  and  $\text{Al}(\text{NO}_3)_3$  films after coating were 0.3 nm, 1.3 nm, reducing to 0.14 nm, 0.18 nm, respectively, after the UV-assisted annealing process. The latter values are comparable to those of the silicon substrate. It is, of course, essential to have a smooth surface in order to achieve reliable device performance; a rough surface will induce a high density of electrical trapping sites or defects, resulting in inferior electronic behaviour.<sup>[1, 7]</sup>

To investigate the electrical properties of our dielectric layers, metal-insulator-semiconductor (MIS) structures were prepared (on a doped Si substrate) and the capacitance of each sample was measured as given in Figure 6. The normalized capacitances (at 1 kHz) and film thicknesses were: 478 nF/cm<sup>2</sup>, 28 nm ( $\text{ZrO}_2$ ); 104 nF/cm<sup>2</sup>, 59 nm ( $\text{Al}_2\text{O}_3$ ); 279 nF/cm<sup>2</sup>, 39 nm ( $\text{ZrO}_2/\text{Al}_2\text{O}_3\text{-F}$ ). (The samples  $\text{ZrO}_2/\text{Al}_2\text{O}_3\text{-F}$  has an  $\text{Al}_2\text{O}_3$  adhesion layer on the bottom electrode, which was prepared from 2%  $\text{Al}(\text{OH})_3$ /formic acid solution – see Table 2, later). All the measured values reveal a frequency dependence, with the capacitance reducing by a factor of 10-30% as the frequency is increased from 100 Hz to 1 MHz; this is comparable to the frequency dispersion reported for similar dielectrics.<sup>[12, 17]</sup> The dielectric constants, obtained using the measured film thicknesses, are shown in Figure 7. The value for  $\text{ZrO}_2$  is

14.6 at 1 kHz, which is within the range of previously reported values, whereas the figure obtained for  $\text{ZrO}_2/\text{Al}_2\text{O}_3\text{-F}$  is 12.3 as a result of the presence of the  $\text{Al}_2\text{O}_3$  adhesion layer. Using the thickness of the  $\text{Al}_2\text{O}_3$  adhesion layer (16 nm), the true dielectric constant of  $\text{ZrO}_2$  may be estimated using the serial capacitance:  $1/C_{\text{observed}} = 1/C_{\text{Al}_2\text{O}_3} + 1/C_{\text{ZrO}_2}$ . The calculated dielectric constant of  $\text{ZrO}_2$  is represented as  $\text{ZrO}_2^{\text{calc}}$  in Table 1 and is 19.8, which is slightly higher than that of our observed  $\text{ZrO}_2$ . Literature dielectric constants for  $\text{ZrO}_2$  are 12 using sol-gel processing;<sup>[31]</sup> 14-19 by CVD;<sup>[32, 33]</sup> 12.5-17.5 by spray pyrolysis;<sup>[34]</sup> and 18-53 by RF sputtering.<sup>[35]</sup> The fact that the value of  $k$  obtained here is in the range reported for solution processing but is somewhat different to values reported for the crystalline phase  $\text{ZrO}_2$  may result from the imperfect densification and from the amorphous nature of our  $\text{ZrO}_2$ . In the case of  $\text{Al}_2\text{O}_3$ , the  $k$  value of our sample is 7.04 at 1 kHz, which is at the lower end range of the literature values.<sup>[36, 37]</sup>

Typical leakage current behavior for the  $\text{ZrO}_2$  and  $\text{Al}_2\text{O}_3$  samples is given in [Figure 8](#); the inset shows the currents measured at different locations across a  $\text{ZrO}_2/\text{Al}_2\text{O}_3\text{-F}$  sample. The majority of devices possessed leakage currents below  $10^{-9}$  A/cm<sup>2</sup> at an applied electric field of 1 MV/cm; the breakdown fields for  $\text{ZrO}_2$ ,  $\text{ZrO}_2/\text{Al}_2\text{O}_3\text{-F}$  and  $\text{Al}_2\text{O}_3$  were approximately 3.5, 2.5 and 8 MV/cm, respectively. These electrical characteristics are the best currently reported for films deposited by solution processing.

[Figure 9](#) shows the output and transfer characteristics of a ZnO TFT using the  $\text{ZrO}_2/\text{Al}_2\text{O}_3$  dielectric, processed with UV exposure at 150 °C. During the device fabrication with the Al gate electrode, it was noted that the dielectric coating was irregular and irreproducible. To improve the coating quality, a 2 wt%  $\text{Al}(\text{OH})_3$  solution, dissolved in formic acid ( $\text{HCOOH}$ ) (in fact, soluble aluminum formate or aluminum hydroxy formate are formed), was spin-coated on a 300 nm  $\text{SiO}_2/\text{Si}$  substrate with Al gate electrodes (see [Figure S6](#)); the substrate



was then heated and exposed to UV for 30 mins at 150 °C. This pre-treatment enhanced considerably the quality of the ZrO<sub>2</sub> dielectric layer. It is thought that Al(OH)<sub>3</sub> becomes soluble in formic acid due to its amphoteric nature. Subsequently, aluminum formate will form during the spin coating, which serves as an interfacial adhesion layer after the UV decomposition process. Since the resulting aluminum formate has an absorption peak at 220 nm, it will be transformed into Al<sub>2</sub>O<sub>3</sub> using a 150 °C UV annealing step. The dielectric characteristics of an Al<sub>2</sub>O<sub>3</sub> film formed from 2 wt% Al(OH)<sub>3</sub> solution are provided in Table 2. As a dielectric layer, the performance of the Al<sub>2</sub>O<sub>3</sub> film formed from a 2 wt% Al(OH)<sub>3</sub> solution is not as good as that of the Al<sub>2</sub>O<sub>3</sub> film formed from Al(NO<sub>3</sub>)<sub>3</sub> solution due to the relatively low density of the film.

A 12.9 wt% ZrO(NO<sub>3</sub>)<sub>2</sub> solution was over-coated on the Al<sub>2</sub>O<sub>3</sub> adhesion layer and subsequently prebaked and UV-assisted thermally annealed for 30 min, as described in Table 1. The TEM image shown in Figure 10 reveals the quality of the Al<sub>2</sub>O<sub>3</sub> and ZrO<sub>2</sub> layers. The Al<sub>2</sub>O<sub>3</sub> layer adheres very well to the Al electrode and the interface between Al<sub>2</sub>O<sub>3</sub> and ZrO<sub>2</sub> layers appears clean and smooth without any visual defects. On the top of the dielectric layer as shown in Figure 10, a 2 wt% Zn(OH)<sub>2</sub>/NH<sub>4</sub>OH solution was spin-coated once at 4000 rpm for 30 sec. Our Zn(OH)<sub>2</sub> is more soluble than commercial material - up to 5 wt%.<sup>[38, 39]</sup> Previous work using commercial samples of ZnO or Zn(OH)<sub>2</sub> has exploited multiple coatings from solution.<sup>[8, 11, 20, 22]</sup> In this respect, our Zn(OH)<sub>2</sub> material is superior in terms of process time and effort. The sample was UV-annealed at 150 °C for 3 min in order to convert the zincate to zinc oxide.<sup>[39]</sup> To complete the ZnO TFT, Al source and drain electrodes were formed using thermal evaporation as shown in Figure S6.

As revealed by Figure 9, the TFTs can be operated at voltages below 3 V. This is attributed directly to the high-k gate dielectric layer ( $k = 12.3$ ) and low thickness of the dielectric layer ( $d \sim 30$  nm). Although our devices were not patterned, the on/off current ratio was about  $4.0 \times 10^6$ , and the threshold voltage ( $V_{th}$ ), subthreshold swing (SS), gate leakage current density ( $I_G$ ) were 0.67 V, 0.08 V/decade and  $10^{-12}$  A/cm<sup>2</sup>. The extracted field-effect mobility in the saturation regime was 1.37 cm<sup>2</sup>/V.s, which is three times higher than the value exhibited by TFTs fabricated using a zirconium acetylacetonate precursor solution as the dielectric layer.<sup>[22]</sup> The observed hysteresis of the transfer curves was about 0.2 V. **This may originate from the hysteresis behavior of the ZrO<sub>2</sub>, as shown in Figure S7, or from the ZnO layer itself.** Lin et al.<sup>[11]</sup> have reported negligible hysteresis of ZnO TFTs using ZrO<sub>2</sub>/Al<sub>2</sub>O<sub>3</sub> bilayer dielectrics under high vacuum. However, considering our TFTs possessed no passivation layer and that the measurements were undertaken in ambient conditions, such a level of hysteresis is acceptable in our preliminary transistors.

Xu et al.<sup>[22]</sup> have used a ZrO<sub>2</sub> dielectric, using a zirconium acetylacetonate precursor, for a ZnO TFT and the same method has been reported by Lin et al.,<sup>[11]</sup> with a minor change to overcome gate leakage. According to the former workers,<sup>[20]</sup> the off-current density of the ZnO TFT is the order of  $10^{-10}$  A/cm<sup>2</sup> at 0.5 V, rising to  $10^{-9}$  A/cm<sup>2</sup> at 3 V. This should be compared to a figure of about  $10^{-12}$  A/cm<sup>2</sup> for the off-current density (two orders of magnitude lower) in our devices. Lin et al.<sup>[11]</sup> have exploited an Al<sub>2</sub>O<sub>3</sub>/ZrO<sub>2</sub> bilayer in order to improve their TFTs. However, this approach requires a lengthy UV exposure (9 hours) to form the Al<sub>2</sub>O<sub>3</sub> layer on the Al electrode. One of the main problems of solution processes is how to control the gate leakage current. Since the passage of leakage currents is mainly through defects or ionic impurities, dielectrics usually require a minimum thickness; otherwise the leakage current behavior is unpredictable. One of the main disadvantages of metal acetylacetonate for dielectric application is the excessive volume shrinkage; following

annealing, the remaining film is only about 20% of its original value. This leads to defective nano-pores, giving significant leakage currents ( $\sim 10^{-5}$  A/cm<sup>2</sup>).<sup>[12, 22]</sup> In the case of our nitrate system, the overall volume change leads to low off-currents and high on/off ratios compared to other reports.<sup>[11, 12, 22]</sup>

In summary, a new low-temperature, solution-processed dielectric formation procedure has been designed and successfully demonstrated. The method is based on the use of metal nitrate salts as precursors, with film processing at 150 °C and under UV irradiation. In principle, this approach can be used to convert any metal nitrate salt to an oxide film. Consequently, it can be used as a versatile tool for many low-temperature oxide film applications, such as gate insulators in thin film transistors. As test systems, ZrO<sub>2</sub> and Al<sub>2</sub>O<sub>3</sub> insulating layers were successfully prepared and their dielectric properties measured. Using **ellipsometric analysis**, **the averaged void concentrations are estimated to be about 15% for the ZrO dielectrics and 25% for the Al<sub>2</sub>O<sub>3</sub> dielectrics**. The leakage currents densities of ZrO<sub>2</sub> and Al<sub>2</sub>O<sub>3</sub> dielectrics are less than about 10<sup>-9</sup> A/cm<sup>2</sup> at 1 MV/cm, which are better than those reported for metal acetylacetonate systems and are comparable to those formed by annealing at high temperature. A ZnO-based TFT was fabricated using the ZrO<sub>2</sub> gate insulator. This device could be operated at less than 3 V and exhibited excellent electrical characteristics **with a mobility of 1.37 cm<sup>2</sup>/V.s and an off-current density of 10<sup>-12</sup> A/cm<sup>2</sup>**. Moreover, since the highest process temperature used was around 150 °C, our device fabrication process is compatible with plastic substrates. These results augur very well for the commercial development of metal oxide thin film transistors. Metal nitrate systems other than ZrO<sub>2</sub> and Al<sub>2</sub>O<sub>3</sub> are under currently investigation.

## Experimental Section

*Solution and film preparation:*

ZrO(NO<sub>3</sub>)<sub>2</sub> and Al(NO<sub>3</sub>)<sub>3</sub> were purchased from Aldrich and used as received. Al(OH)<sub>3</sub> was prepared in our laboratory by titrating aqueous 0.1 M Al(NO<sub>3</sub>)<sub>3</sub> with ammonia water. Subsequently, the gel-like Al(OH)<sub>3</sub> product was filtered and washed several times with deionized water. The ZrO(NO<sub>3</sub>)<sub>2</sub> and Al(NO<sub>3</sub>)<sub>3</sub> stock solutions were prepared in water and 2-methoxyethanol, respectively, and a co-solvent was added to a given stock solution according to Table 1 in order to improve the film quality. The resulting solution was filtered using a 0.2 μm membrane filter and spin-coated at a speed of 4000 rpm for 30 s on a p-doped Si substrate for dielectric measurements. The coated films were pre-annealed at 80 °C and then heated to 150 °C according to Table 1. To prepare metal oxide dielectrics from the precursor, UV exposure at 150 °C was undertaken for 20 to 30 min in air. For this purpose, a 1.1 kW medium pressure mercury UV lamp (Lichtzen, Korea), with a peak intensity at 365 nm and broad bands between 320 nm and 200 nm, was used. The sample to lamp distance was set to 10 cm. For capacitance and leakage current measurements, 0.65 mm<sup>2</sup> Al electrodes were deposited on the dielectric film using a thermal evaporator (DAEKI HI-TECH Co.) to form MIS (metal-insulator-semiconductor) structures. To make a bottom-gate, top-contact ZnO TFT architecture, Al gate electrodes were first formed by thermal evaporation on a 300 nm SiO<sub>2</sub>/p-doped Si wafer. A 2 wt% Al(OH)<sub>3</sub>/formic acid solution was used as an adhesion layer and the dielectric film was then deposited by the method described above. Following UV calcination of the dielectric film at 150 °C, a 2 wt% Zn(OH)<sub>2</sub> solution<sup>[38, 39]</sup> in ammonia water was spin-coated and then converted to ZnO by UV exposure for 3 min at 150 °C. The transistor device was completed by source and drain electrodes, prepared by thermally evaporating aluminum; the TFT channel width was 200 μm with a length of 40 μm.

*Measurement and Analysis:*

A surface profilometer (Kosaka ET-3000) or FE-SEM (Carl Zeiss LEO SUPRA 55) were used to measure the film thicknesses. **For film characterization, ellipsometer (V-Vase ellipsometer, J. A. Woollam) with WVASE32 software was used.** Surface roughnesses were obtained using an Atomic Force Microscope (N8 ARGOS, Bruker-Nano, Germany). Capacitance measurements were undertaken using an Agilent 4284A LCR meter. The TFT performance and leakage measurements were performed, in ambient air, by a semiconductor parameter analyzer (Agilent 4156C). Field emission scanning electron microscopy (FE-SEM) and high resolution transmission electron microscopy (HR-TEM) images were taken to monitor the film qualities. X-ray Photoelectron Spectroscopy (XPS) (K-Alpha, Thermo Electron) was used to identify the relative oxygen vacancies in the dielectric films.

### Supporting Information

Supporting Information is available from the Wiley Online Library or from the author.

### Acknowledgements

This work is supported by National Research Foundation of Korea (grant #: NRF-2012R1A1A2003620) and Ministry of Trade, Industry & Energy of Korea (grant #: 10041808). J. Hwang and K. Lee equally contributed as first author to this work.

Received: ((will be filled in by the editorial staff))

Revised: ((will be filled in by the editorial staff))

Published online: ((will be filled in by the editorial staff))

### References

- [1] J. F. Wager, D. A. Keszler, R. E. Presley, *Transparent Electronics*, Wiley, New York, U.S.A. **2008**.
- [2] A. Facchetti, T. J. Marks, Eds, *Transparent Electronics: From Synthesis to Applications*, Wiley, Chichester, UK **2010**.
- [3] E. Fortunato, P. Barquinha, R. Martins, *Adv Mater.* **2012**, 24(22), 2945-2986.

- [4] K. K. Banger, Y. Yamashita, K. Mori, R. L. Peterson, T. Leedham, J. Rickard, H. Siringhaus, *Nat Mater.* **2011**, *10*(1), 45-50.
- [5] K. K. Banger, R. L. Peterson, K. Mori, Y. Yamashita, T. Leedham, H. Siringhaus, *Chem. Mater.* **2013**.
- [6] P. Barquinha, L. Pereira, G. Goncalves, D. Kuscer, M. Kosec, A. Vila, A. Olziersky, J. R. Morante, R. Martins, E. Fortunato, *J. Soc. Inf. Disp.* **2010**, *18*(10), 762-772.
- [7] G. D. Wilk, R. M. Wallace, J. M. Anthony, *J. Appl. Phys.* **2001**, *89*(10), 5243-5275.
- [8] T. Jun, K. Song, Y. Jeong, K. Woo, D. Kim, C. Bae, J. Moon, *J. Mater. Chem.* **2011**, *21*(4), 1102-1108.
- [9] S. Jeong, J. Moon, *J. Mater. Chem.* **2011**, *22*, 1243-1250.
- [10] Y. Kim, J. Heo, T. Kim, S. Park, M. Yoon, J. Kim, M. S. Oh, G. Yi, Y. Noh, S. K. Park, *Nature (London, U. K. )*. **2012**, *489*(7414), 128-132.
- [11] Y. Lin, H. Faber, K. Zhao, Q. Wang, A. Amassian, M. McLachlan, T. D. Anthopoulos, *Adv Mater.* **2013**, *25*(31), 4340-4346.
- [12] Y. M. Park, A. Desai, A. Salleo, L. Jimison, *Chem. Mater.* **2013**, *25*(13), 2571-2579.
- [13] S. Y. Lee, S. Chang, J. Lee, *Thin Solid Films.* **2010**, *518*(11), 3030-3032.
- [14] J. Robertson, *The European Physical Journal - Applied Physics.* **2004**, *28*(03), 265-291.
- [15] S. J. Wang, T. I. Wong, Q. Chen, M. Yang, L. M. Wong, J. W. Chai, Z. Zhang, J. S. Pan, Y. P. Feng, *Physica Status Solidi (A)*. **2010**, *207*(7), 1731-1734.
- [16] R. P. Ortiz, A. Facchetti, T. J. Marks, *Chem. Rev.* **2010**, *110*(1), 205-239.

- [17] G. Adamopoulos, S. Thomas, P. H. Wöbkenberg, D. D. C. Bradley, M. A. McLachlan, T. D. Anthopoulos, *Adv Mater.* **2011**, 23(16), 1894-1898.
- [18] K. M. Kim, C. W. Kim, J. Heo, H. Na, J. E. Lee, C. B. Park, J. Bae, C. Kim, M. Jun, Y. K. Hwang, S. T. Meyers, A. Grenville, D. A. Keszler, *Appl. Phys. Lett.* **2011**, 99(24).
- [19] G. Adamopoulos, S. Thomas, D. D. C. Bradley, M. A. McLachlan, T. D. Anthopoulos, *Appl. Phys. Lett.* **2011**, 98(12).
- [20] S. T. Meyers, J. T. Anderson, C. M. Hung, J. Thompson, J. F. Wager, D. A. Keszler, *J. Am. Chem. Soc.* **2008**, 130(51), 17603-17609.
- [21] Y. M. Park, J. Daniel, M. Heeney, A. Salleo, *Adv Mater.* **2011**, 23(8), 971-974.
- [22] X. Xu, Q. Cui, Y. Jin, X. Guo, *Appl. Phys. Lett.* **2012**, 101(22).
- [23] L. Pereira, H. Aguas, E. Fortunato, R. Martins, *Appl. Surf. Sci.* **2006**, 253(1), 339-343.
- [24] A. D. Walsh, *J. Chem. Soc.* **1953**, 2301-6.
- [25] G. P. Smith, C. R. Boston, *J. Chem. Phys.* **1961**, 34(4), 1396-1406.
- [26] A. Mookherji, S. P. Tandon, *Indian J. Phys.* **1962**, 36, 344-50.
- [27] N. S. Bayliss, R. B. Bucat, *Aust. J. Chem.* **1975**, 28(9), 1865-1878.
- [28] J. Mack, J. R. Bolton, *J. Photochem. Photobiol. A.* **1999**, 128(1-3), 1-13.
- [29] S. Goldstein, J. Rabani, *J. Am. Chem. Soc.* **2007**, 129(34), 10597-10601.
- [30] Y. Z. Hu, S. Tay, *Proc. - Electrochem. Soc.* **2001**, 2001-9, 197-204.

- [31] H. Shimizu, S. Konagai, M. Ikeda, T. Nishide, *Jpn. J. Appl. Phys.* **2009**, 48(10), 101101/1-101101/6.
- [32] M. Balog, M. Schieber, M. Michman, S. Patai, *Thin Solid Films.* **1977**, 47(2), 109-120.
- [33] J. Shappir, A. Anis, I. Pinsky, *Electron Devices, IEEE Transactions on.* **1986**, 33(4), 442-449.
- [34] G. Reyna-Garcia, M. Garcia-Hipolito, J. Guzman-Mendoza, M. Aguilar-Frutis, C. Falcony, *J. Mater. Sci. : Mater. Electron.* **2004**, 15(7), 439-446.
- [35] A. P. Huang, P. K. Chu, H. Yan, M. K. Zhu, *J. Vac. Sci. Technol. , B: Microelectron. Nanometer Struct. Process., Meas. , Phenom.* **2005**, 23(2), 566-569.
- [36] K. Vanbesien, P. De Visschere, P. F. Smet, D. Poelman, *Thin Solid Films.* **2006**, 514(1-2), 323-328.
- [37] C. M. Tanner, Y. Perng, C. Frewin, S. E. Saddow, J. P. Chang, *Appl. Phys. Lett.* **2007**, 91(20).
- [38] H. Kim, J. Hwang, M. Lee, Korean Pat. Appl. 10-2013-0164867, **2013**.
- [39] J. Hwang, J. Park, H. Kim, *Semicon. Sci. Technol. , submitted.*



## Figure and Table Captions

**Figure 1.** Film thickness dependence of zirconium oxynitrate and aluminum nitrate as a function of UV irradiation time. Fitting results are using  $z=y_0+A \exp(-T/t)$ .  $ZrO_2^*$  from Ref. [12]

**Figure 2.** Extracted refractive indices of  $Al_2O_3$  and  $ZrO_2$  films as a function of wavelength, from ellipsometric measurements.

**Figure 3.** XPS data for  $ZrO_2$  and  $Al_2O_3$  prepared from zirconium oxynitrate and aluminum nitrate. Fitting result (green) is overlay on the original data (black). Both sets of results show the hydroxide O1s peaks.

**Figure 4.** Sectional SEM images of  $ZrO_2$  and  $Al_2O_3$  thin films after UV-assisted thermal annealing. A) 16 nm  $Al_2O_3$  film from 2%  $Al(OH)_3$ /formic acid solution, denoted as  $Al_2O_3$ -F, B) 28nm  $ZrO_2$  film from 12.85%  $ZrO(NO_3)_2/H_2O/2ME$  solution, (see Figure S5 for contrast enhanced image), C) 39 nm  $ZrO_2/Al_2O_3$  film from single coating of  $Al_2O_3$ -F and single coating of 12.85%  $ZrO(NO_3)_2/H_2O/2ME$  solution, D) 64 nm  $ZrO_2/Al_2O_3$  film from single coating of  $Al_2O_3$ -F and double coating of 12.85%  $ZrO(NO_3)_2/H_2O/2ME$  solution, E) 116nm  $ZrO_2/Al_2O_3$  film from single coating of  $Al_2O_3$ -F and double coating of 16.34%  $ZrO(NO_3)_2/H_2O/2ME$  solution, F) 59nm  $Al_2O_3$  film from double coating of 11.8%  $Al(NO_3)_3/2ME/H_2O$  solution.

**Figure 5.** AFM images of  $ZrO_2$  and  $Al_2O_3$ . The RMS roughness becomes less following UV annealing.

**Figure 6.** Frequency dependence of unit capacitances of  $ZrO_2$ ,  $ZrO_2/Al_2O_3$ -F,  $Al_2O_3$ , and  $Al_2O_3$ -F.

**Figure 7.** Dielectric constants of  $ZrO_2$ ,  $ZrO_2/Al_2O_3$ -F,  $Al_2O_3$ , and  $Al_2O_3$ -F as a function of frequency.

**Figure 8.** Leakage current density for  $ZrO_2$ ,  $ZrO_2/Al_2O_3$ -F, and  $Al_2O_3$  thin films as a function of the applied electric field using an MIS structure. The inset shows typical leakage current density behavior of  $ZrO_2/Al_2O_3$ -F at different sample locations.

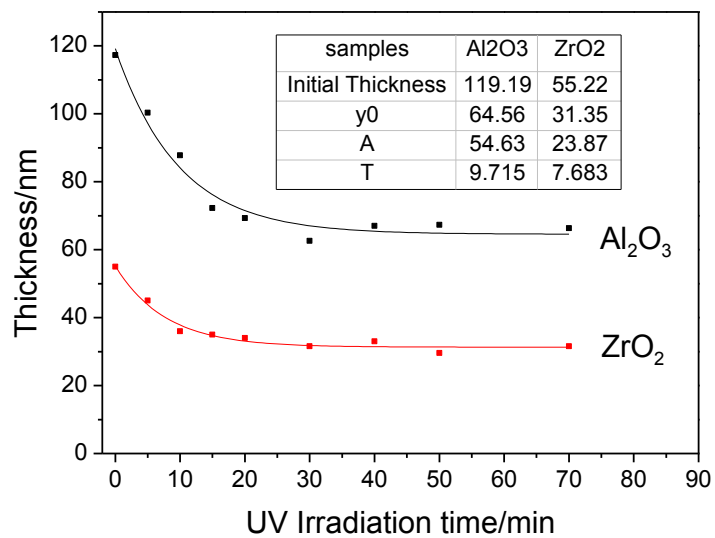
**Figure 9.** Output and transfer characteristics of ZnO TFT using  $ZrO_2/Al_2O_3$ -F dielectric layer. Both the ZnO semiconductor and the  $ZrO_2/Al_2O_3$ -F dielectric layer were processed at 150 °C with UV exposure.

**Figure 10.** TEM image of dielectric layers on Al electrode.

**Table 1.** Summary of ellipsometric analysis of  $ZrO_2$  and  $Al_2O_3$  dielectrics.

**Table 2.** Summary of characteristics of dielectric materials

Figure 1.



Thickness	Al <sub>2</sub> O <sub>3</sub>	ZrO <sub>2</sub>	ZrO <sub>2</sub> *
Observed	54%	57%	22%
Theoretical	24%	53%	25%

Figure 2.

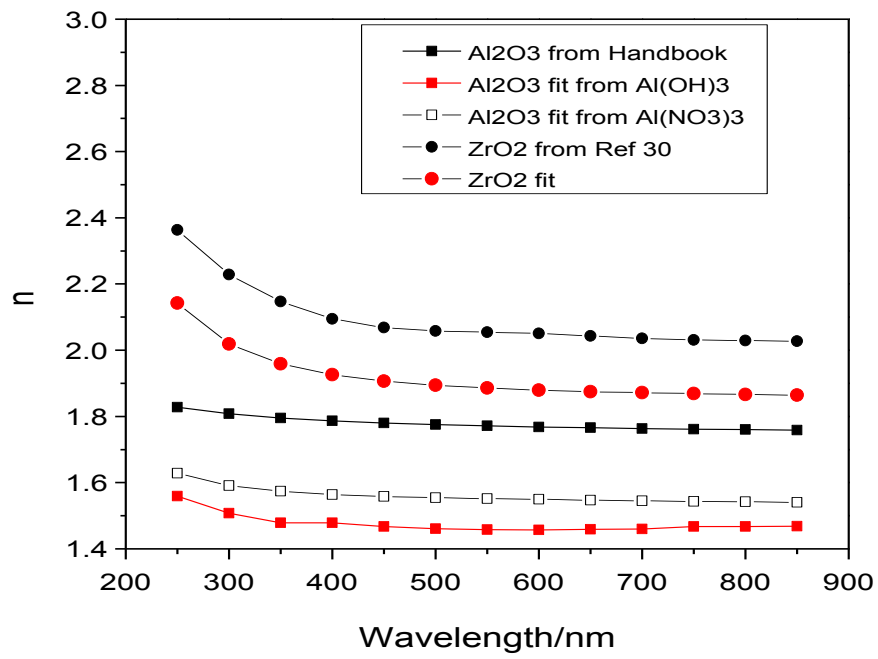


Figure 3.

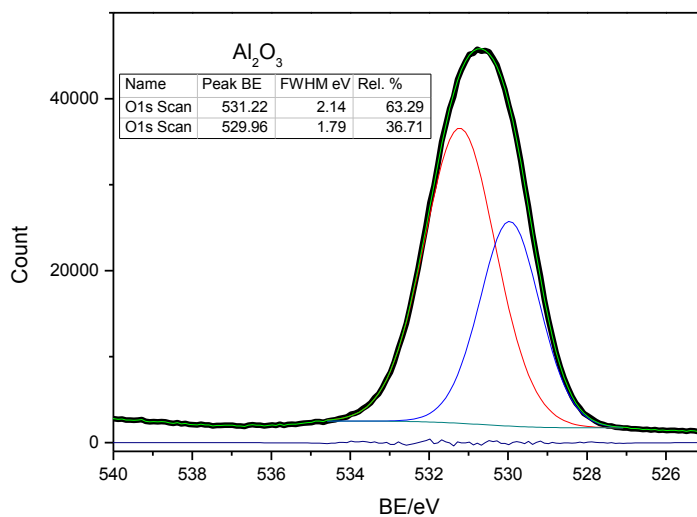
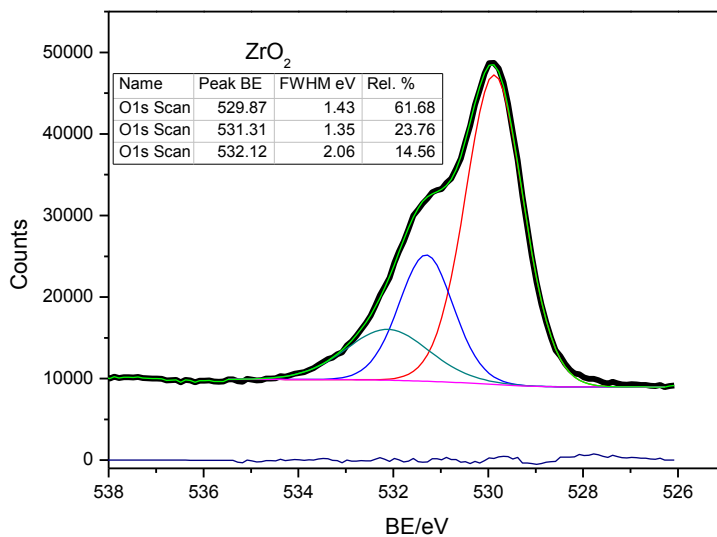


Figure 4.

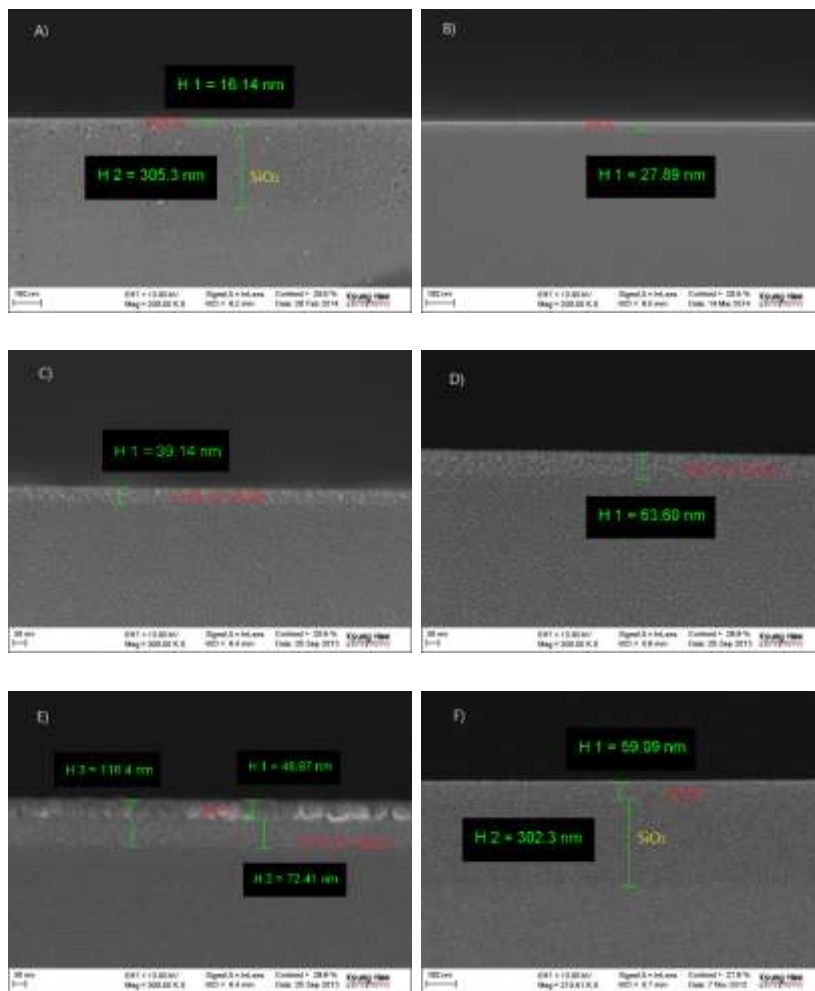


Figure 5.

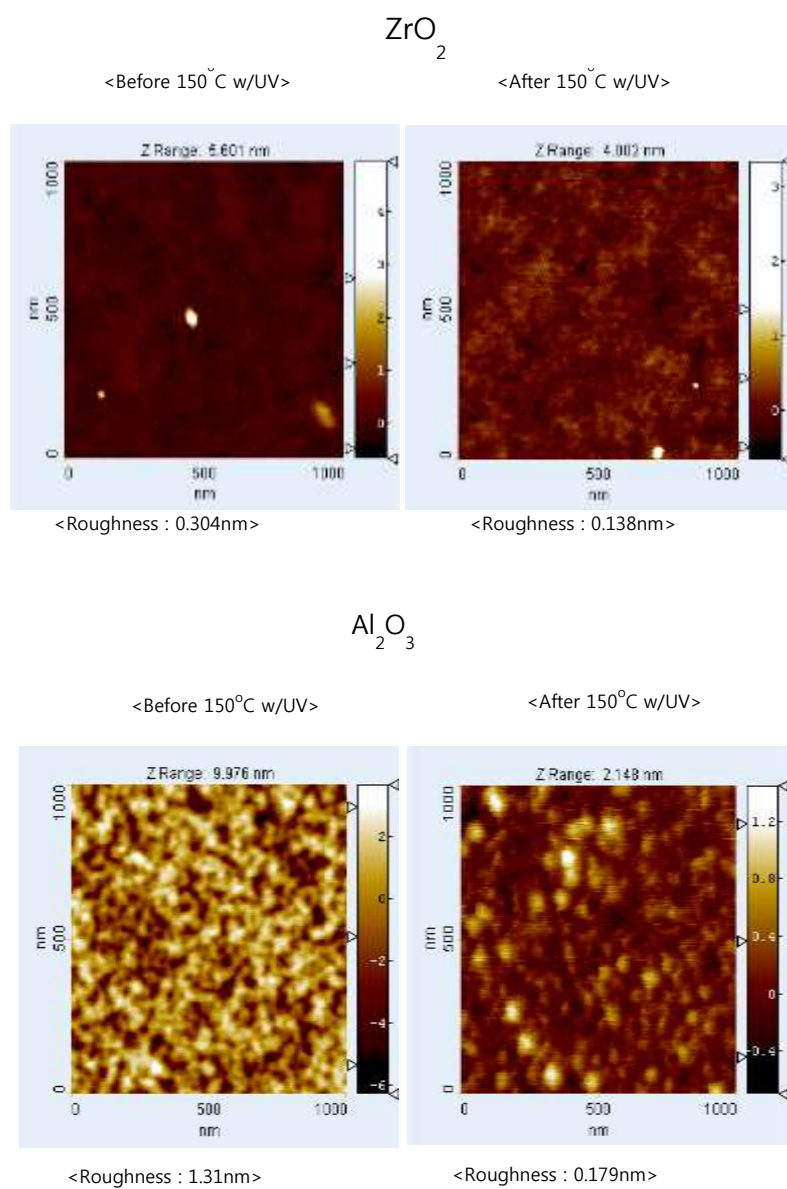


Figure 6.

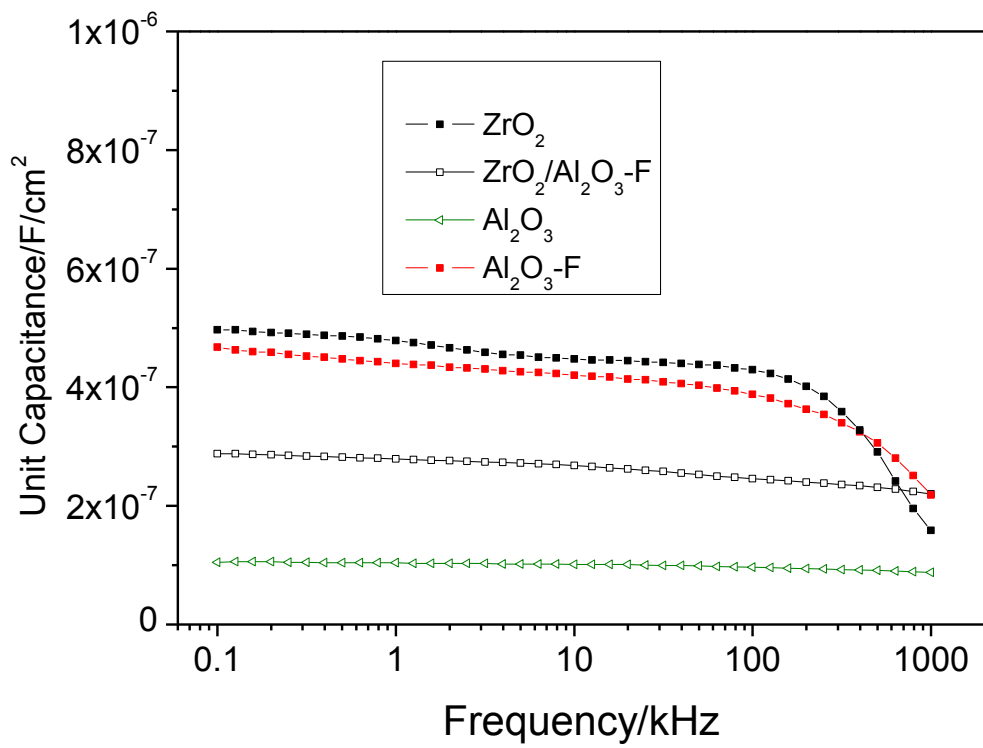


Figure 7.

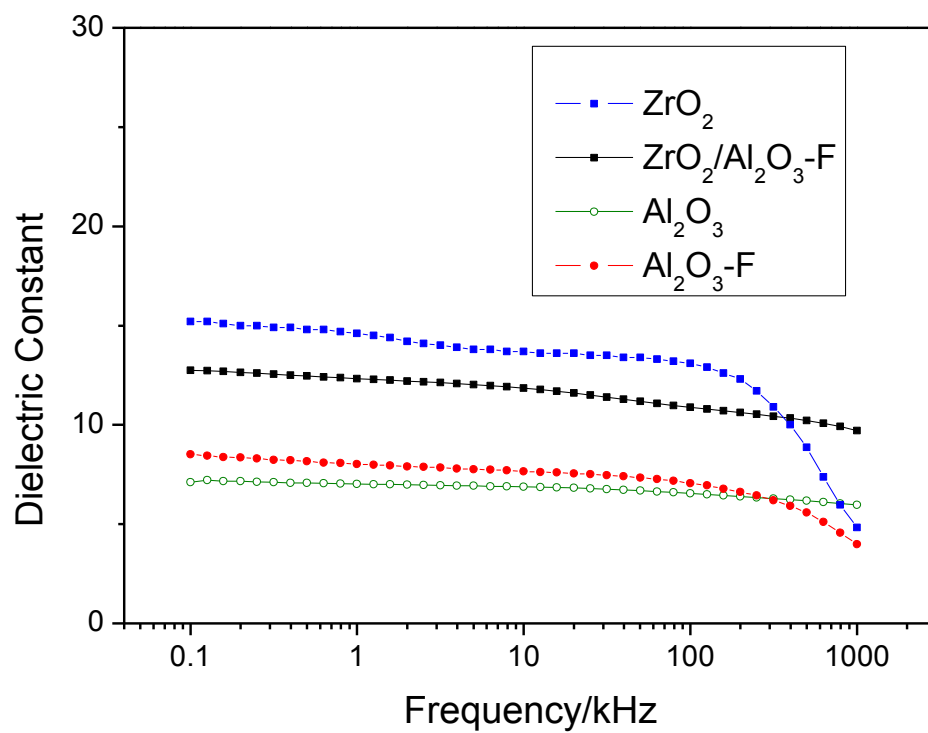




Figure 8.

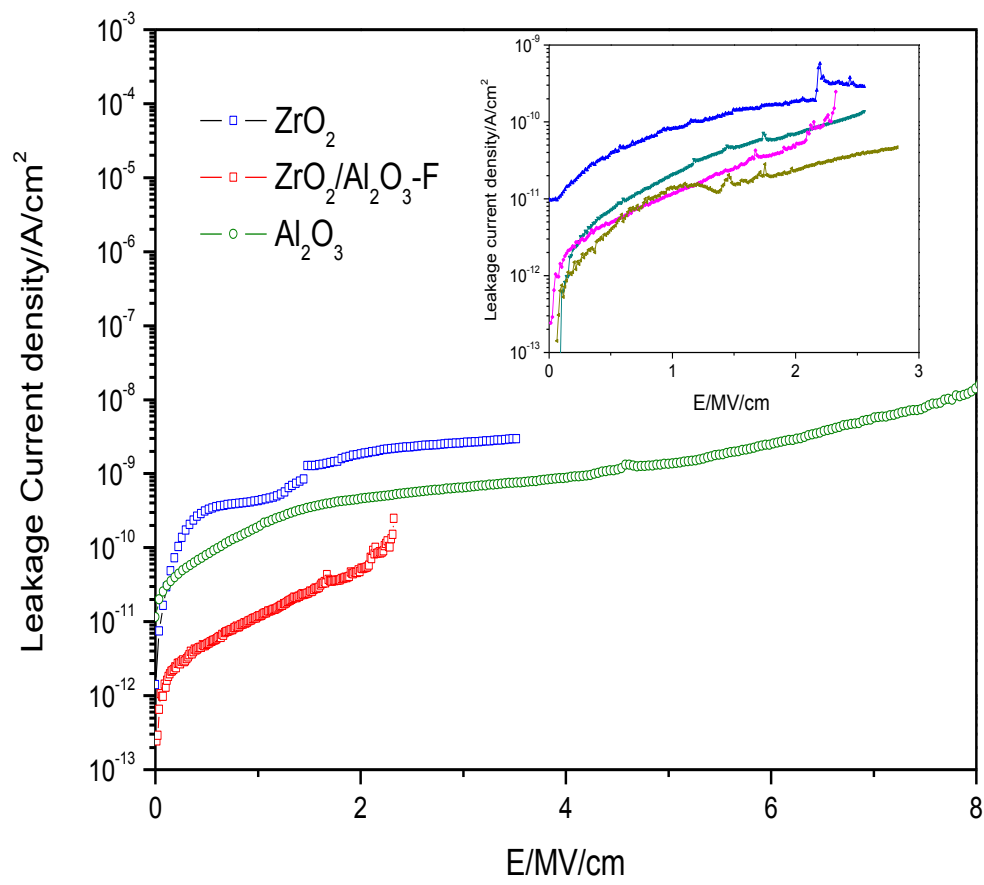


Figure 9.

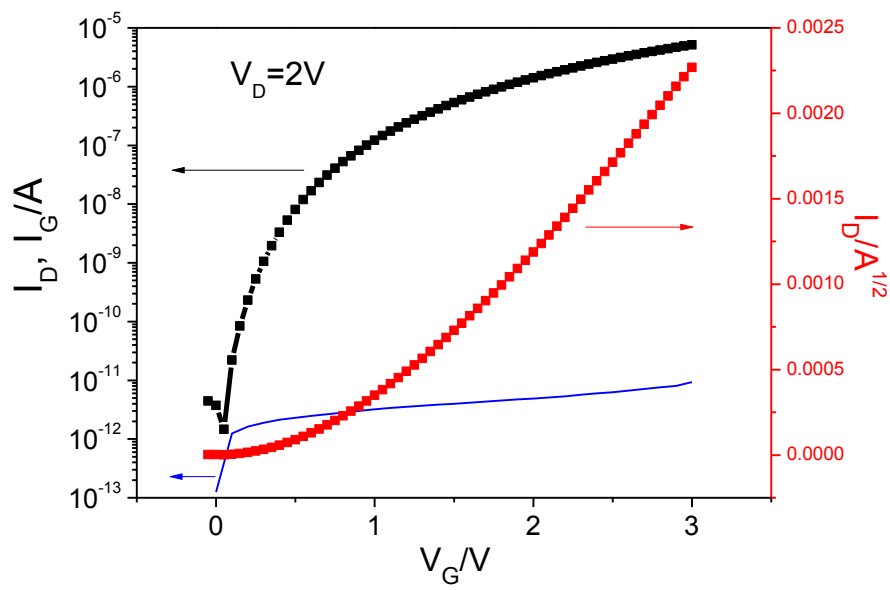
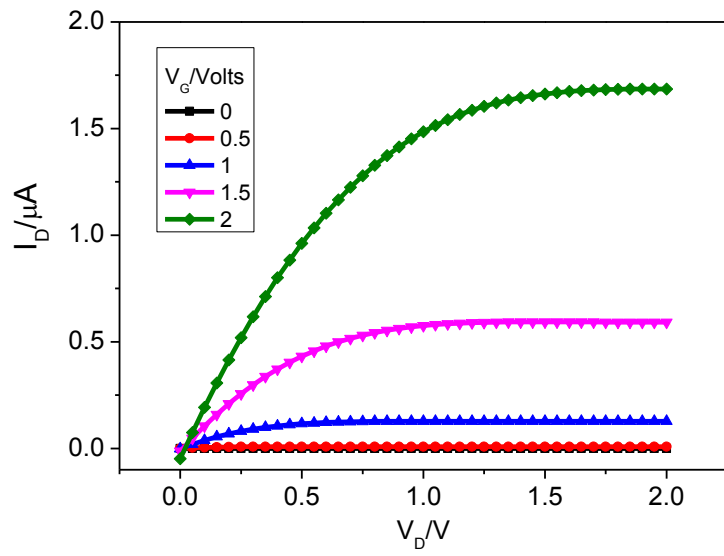
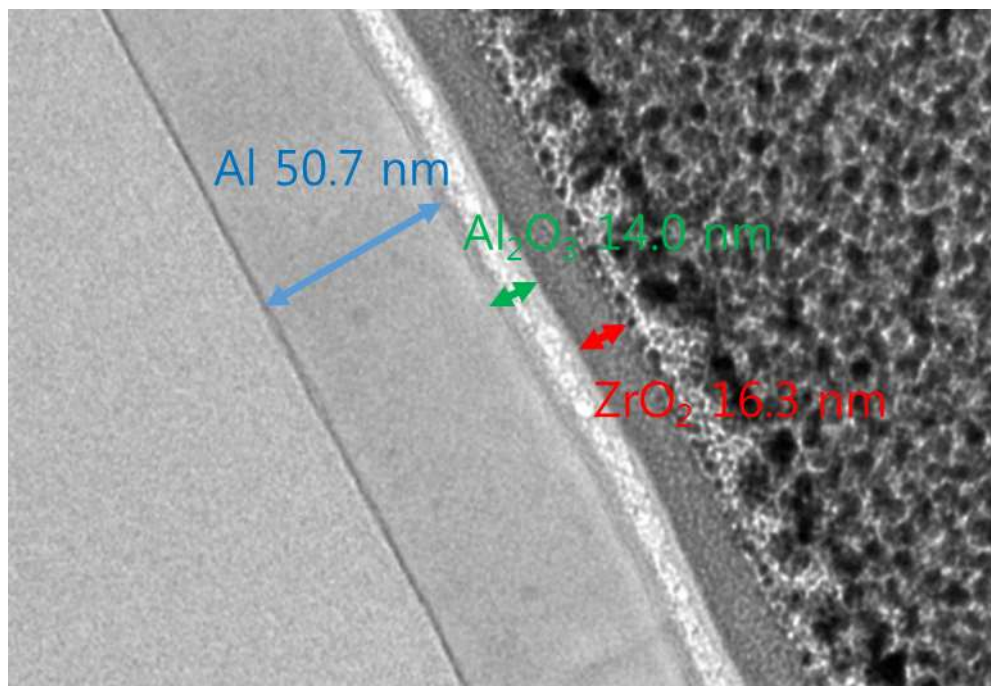


Figure 10.



**Table 1.**

Samples	Precursor	Model	d(ZrO <sub>2</sub> )/nm	d(Al <sub>2</sub> O <sub>3</sub> )/nm	d(SiO <sub>2</sub> )/nm	Void/%	MSE
ZrO <sub>2</sub>	ZrO(NO <sub>3</sub> ) <sub>2</sub>	BME	17.3	-	0.5	15.4	0.6593
		Simple	17.5	-	0.3	-	0.6555
ZrO <sub>2</sub> /Al <sub>2</sub> O <sub>3</sub> bilayer	ZrO(NO <sub>3</sub> ) <sub>2</sub> /Al(OH) <sub>3</sub>	BME	17.8	9	0	15.5(ZrO <sub>2</sub> )/32.0(Al <sub>2</sub> O <sub>3</sub> )	0.8954
		Simple	18.7	7.6	0.5	-	0.8375
Al <sub>2</sub> O <sub>3</sub>	Al(OH) <sub>3</sub>	BME	-	12.2	0.6	33.1	0.2296
		Simple	-	12.4	0.1	-	0.3113
Al <sub>2</sub> O <sub>3</sub> bilayer	Al(NO <sub>3</sub> ) <sub>3</sub>	BME	-	67.6	0	25.7	0.3689
		Simple	-	66.1	0	-	0.5114

Table 2.

Sample	Stock Solution	Co-solvent	Mixing Ratio Stock/Cosolvent	Effective Conc. /Wt%	Layers	Condition Temp./Duration	Co* /nF/cm <sup>2</sup>	Thickness/ nm	Dielectric Constant	Leakage Current Density**	Break-down /MV/cm
ZrO <sub>2</sub>	0.8M ZrO(NO <sub>3</sub> ) <sub>2</sub> /H <sub>2</sub> O	2ME	2/1	12.85	1	80/10min 150/20min 150/UV30min	478	28	14.6	4.30x10 <sup>-10</sup>	3.5
Al <sub>2</sub> O <sub>3</sub>	0.4M Al(NO <sub>3</sub> ) <sub>3</sub> /2ME	H <sub>2</sub> O	4/1	11.8	2	80/30min 150/UV30min	104	59	7.04	2.41x10 <sup>-10</sup>	8
ZrO <sub>2</sub> /Al <sub>2</sub> O <sub>3</sub> -F <sup>†</sup>	0.8M ZrO(NO <sub>3</sub> ) <sub>2</sub> /H <sub>2</sub> O	2ME	2/1	12.85	1	80/10min 150/20min 150/UV30min	279	39	12.3	1.19x10 <sup>-11</sup>	2.3
Al <sub>2</sub> O <sub>3</sub> -F	2% Al(OH) <sub>3</sub> /formic acid	-	-	2	1	80/10min 150/20min 150/UV30min	440	16	8.01	-	-
ZrO <sub>2</sub> <sup>calc</sup>	-	-	-	-	1	-	762	23	19.8	-	-

\* Unit capacitance at 1 kHz

\*\* Leakage Current density (A/cm<sup>2</sup>) at the 1 MV/cm

† after 2% Al(OH)<sub>3</sub>/formic acid solution coating, ZrO<sub>2</sub> layer was prepared

## The table of contents

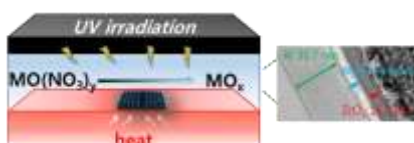
**Solution-based oxide gate dielectric layers** are prepared from metal nitrates using UV-assisted annealing at 150 °C. The leakage current densities of  $\text{ZrO}_2$  and  $\text{Al}_2\text{O}_3$  dielectrics are less than about  $10^{-9} \text{ A/cm}^2$  at 1 MV/cm and comparable to those formed by annealing at higher temperatures. High dielectric constants and the low leakage current behavior of the dielectric layers provide excellent ZnO TFT performance, with a field effect mobility of  $1.37 \text{ cm}^2/\text{V}\cdot\text{s}$  and an off-current density of  $10^{-12} \text{ A/cm}^2$ . This low fabrication temperature process is compatible with future plastic electronics technology.

**Keyword:** UV-assisted annealing, gate insulator, oxide dielectrics, metal nitrate, ZnO TFT

Jaeun Hwang, Kyungmin Lee, Yesul Jeong, Yong Uk Lee, Christopher Pearson, Michael C. Petty and Hongdoo Kim\*

## UV-assisted Low Temperature Oxide Dielectric Films for TFT Applications

**ToC figure** ((Please choose one size: 55 mm broad  $\times$  50 mm high or 110 mm broad  $\times$  20 mm high. Please do not use any other dimensions))



## Supporting Information

**UV-assisted Low Temperature Oxide Dielectric Films for TFT Applications**

*Jaeun Hwang, Kyungmin Lee, Yesul Jeong, Yong Uk Lee, Christopher Pearson,  
Michael C. Petty, Hongdoo Kim\**

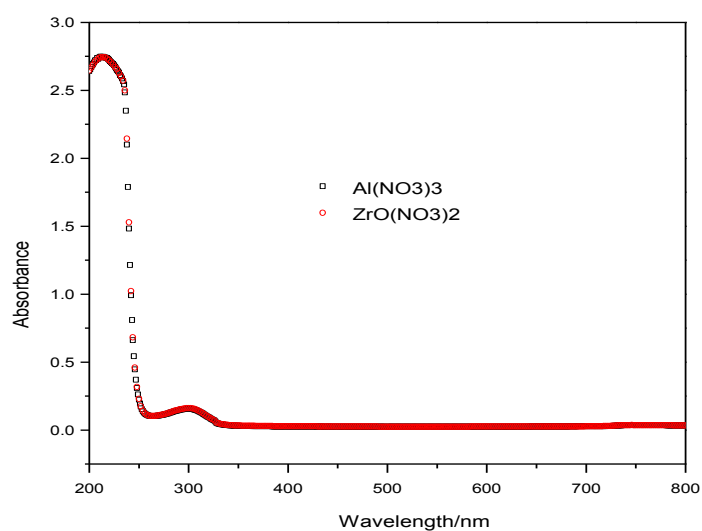


Figure S1. UV spectra of zirconium oxynitrate and aluminum nitrate. The same nitrate concentration gives a similar UV absorption.

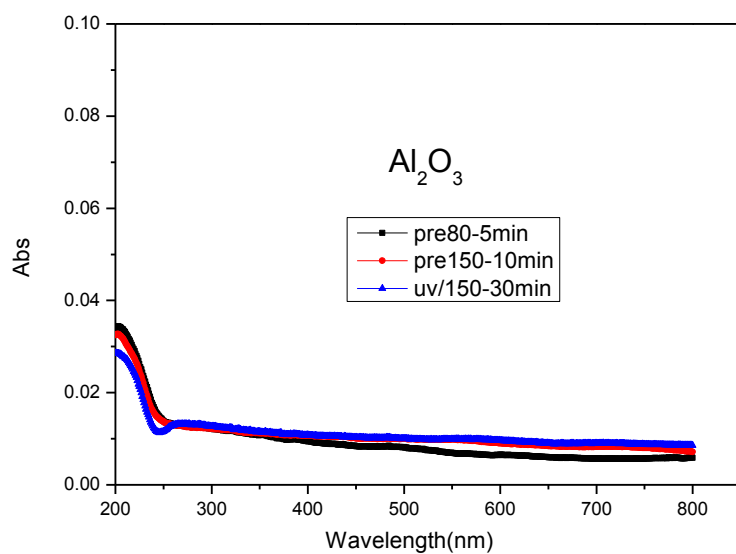
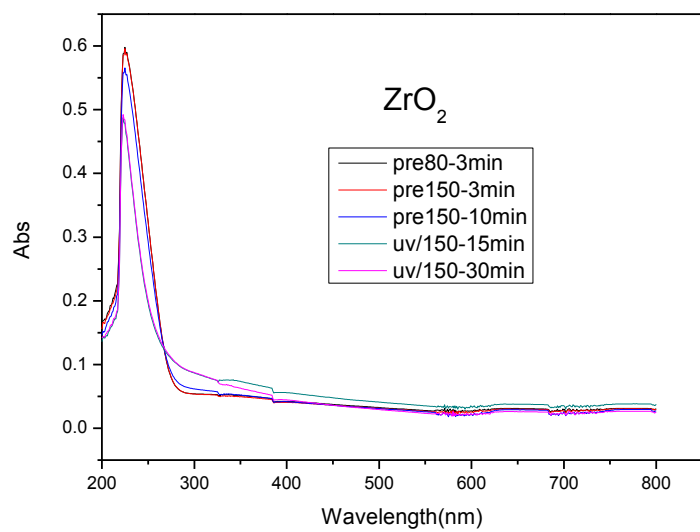
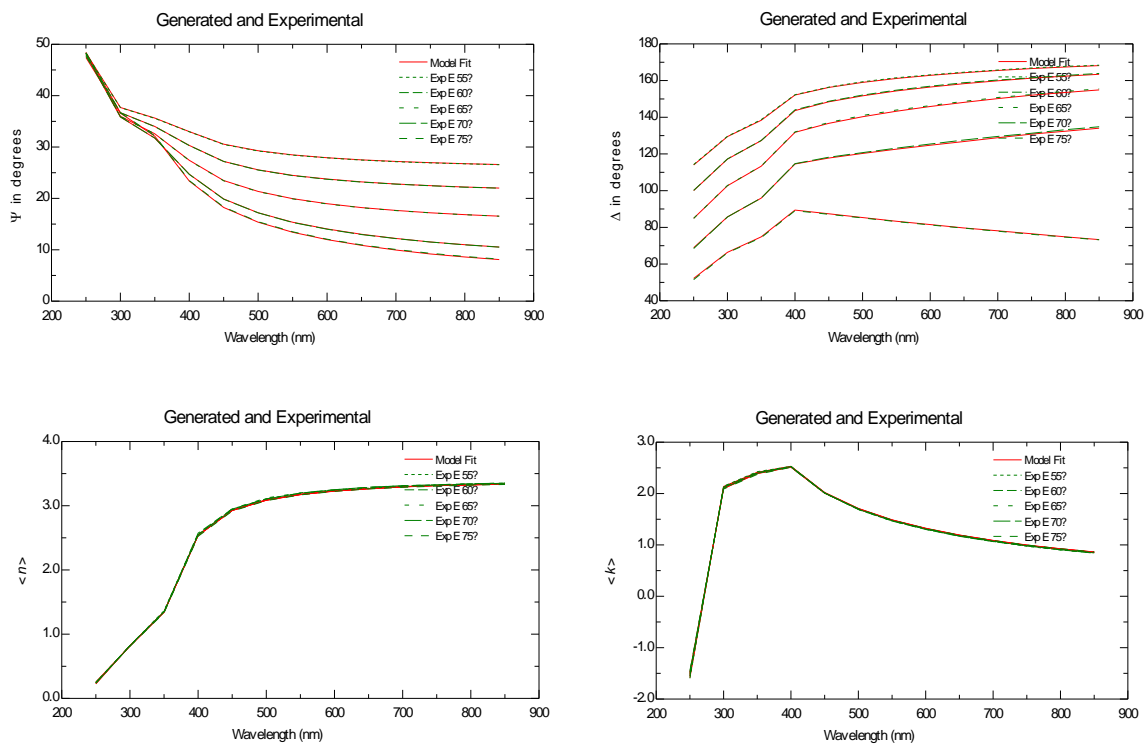


Figure S2. UV/Visible spectra of  $ZrO_2$  and  $Al_2O_3$  deposited on quartz substrates.



Figure S3. Ellipsometric fitting results using WVASE32 program.

A-1) ZrO<sub>2</sub> layer, fitting with EMA model



A-2) ZrO<sub>2</sub> layer, fitting with simple model

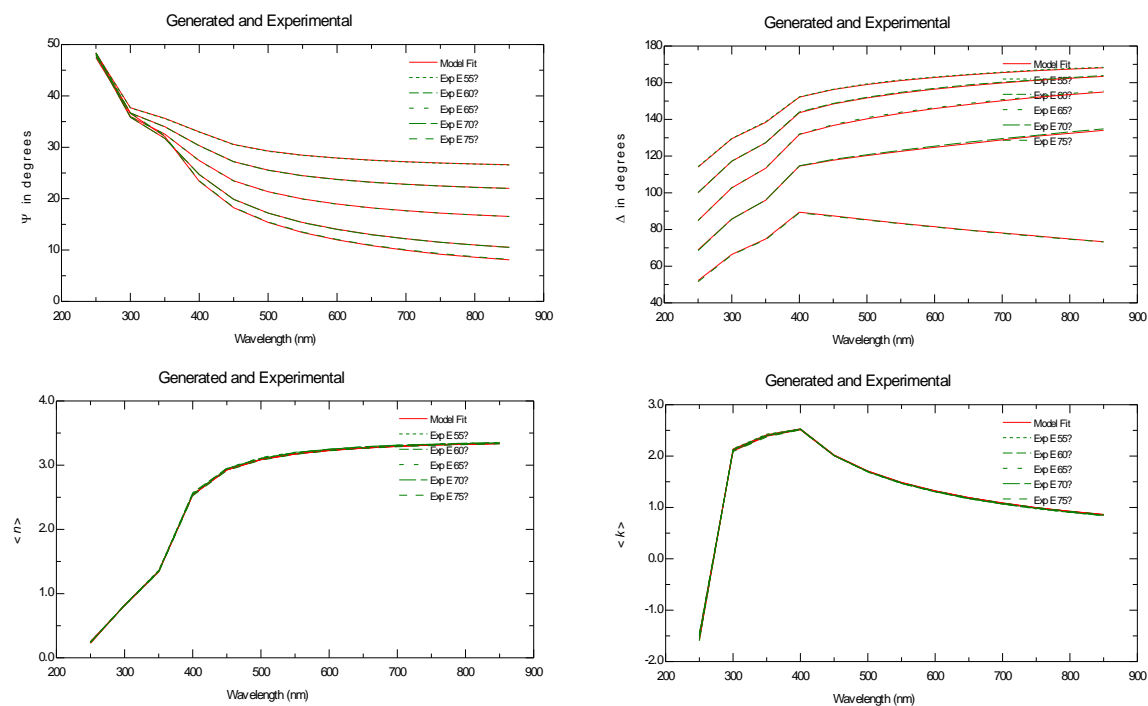
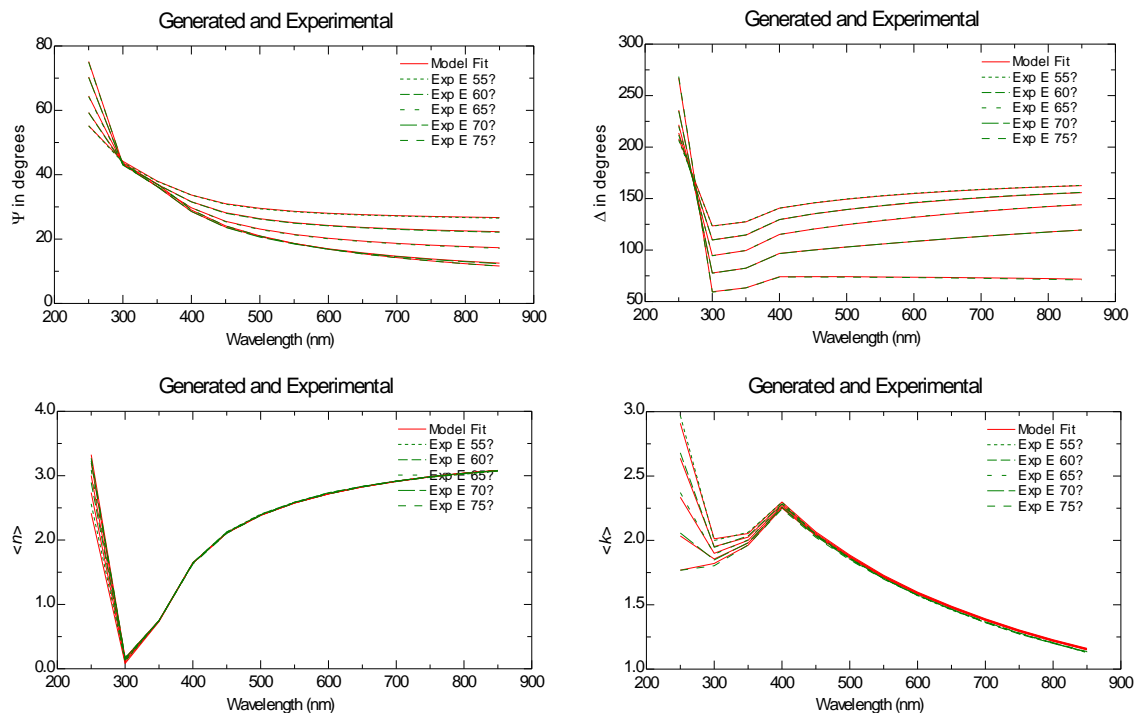


Figure S3. Ellipsometric fitting results using WVASE32 program (continued).

B-1) ZrO<sub>2</sub> with Al<sub>2</sub>O<sub>3</sub> layer, fitting with EMA model



B-2) ZrO<sub>2</sub> with Al<sub>2</sub>O<sub>3</sub> layer, fitting with simple model

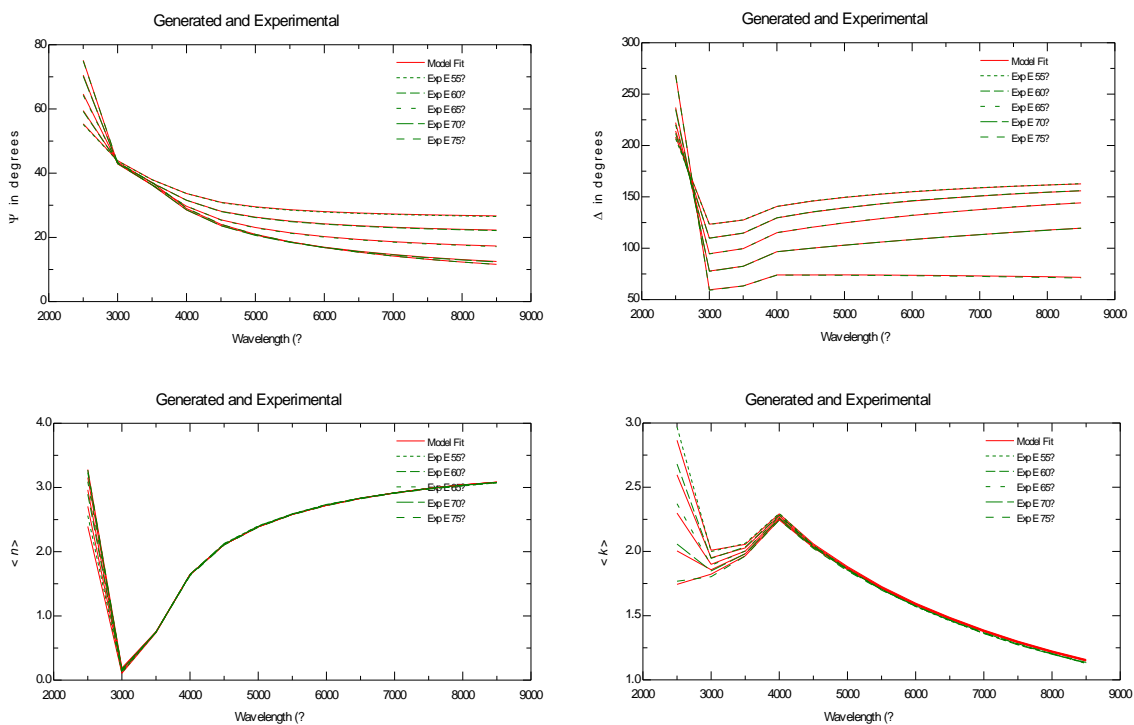
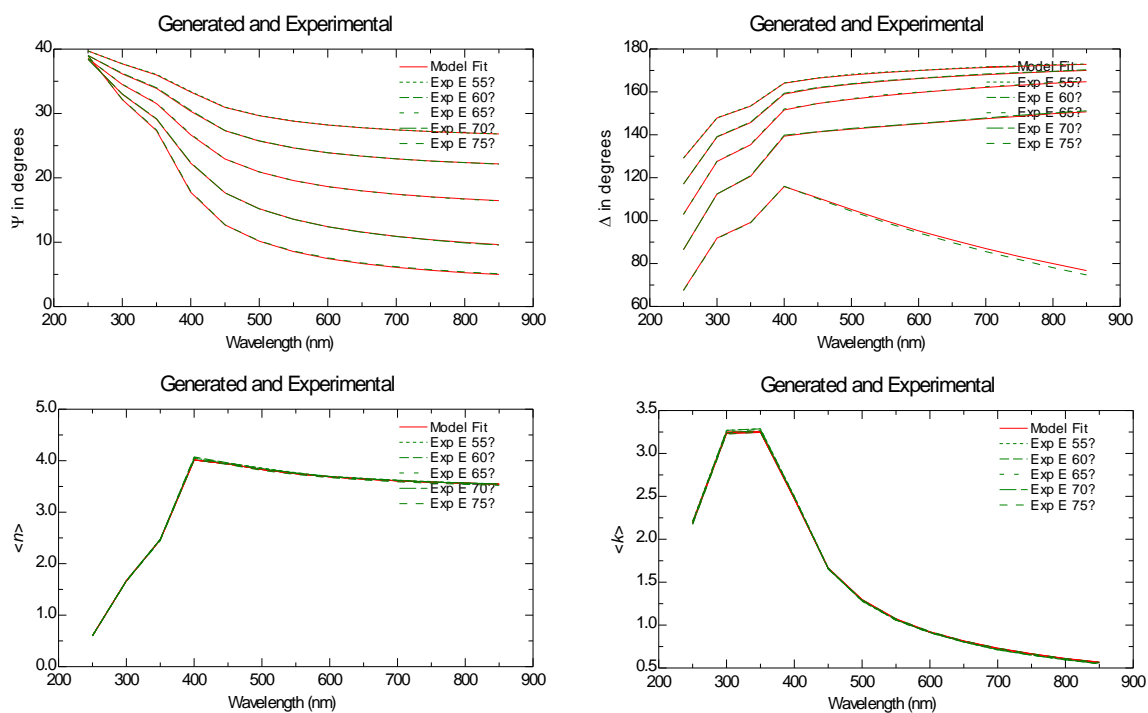


Figure S3. Ellipsometric fitting results using WVASE32 program (continued).

C-1) Al<sub>2</sub>O<sub>3</sub> layer from Al(OH)<sub>3</sub>, fitting with EMA model



C-2) Al<sub>2</sub>O<sub>3</sub> layer from Al(OH)<sub>3</sub>, fitting with simple model

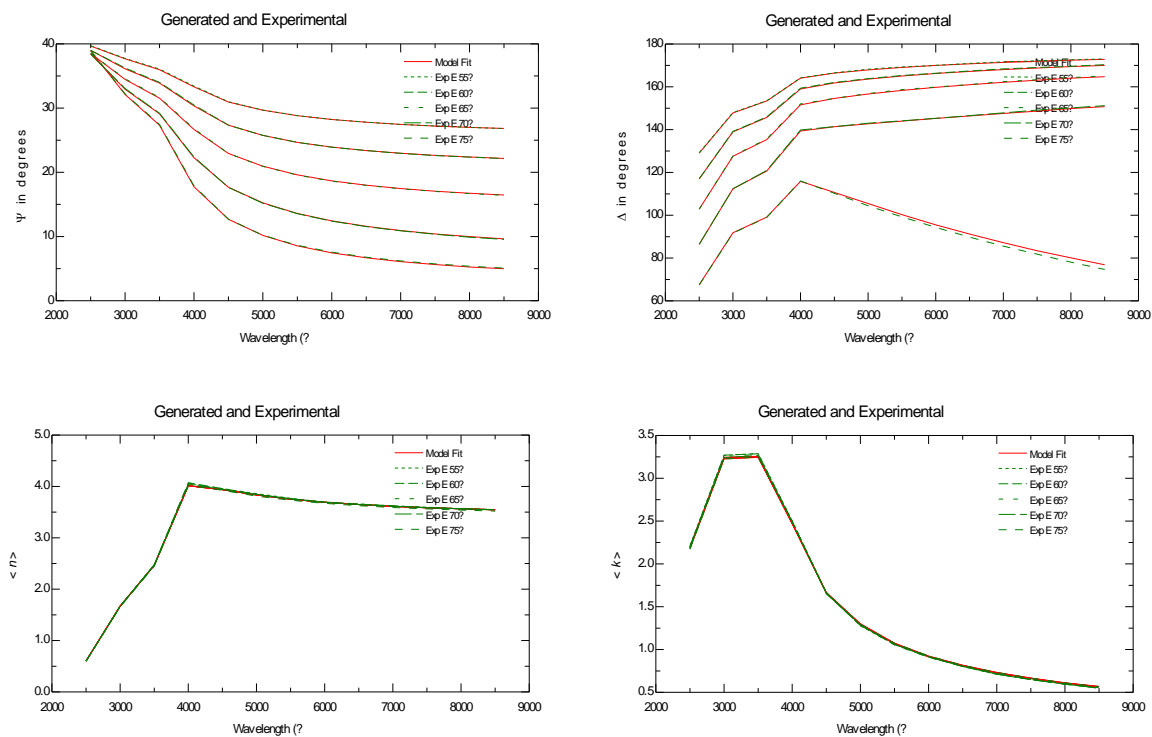
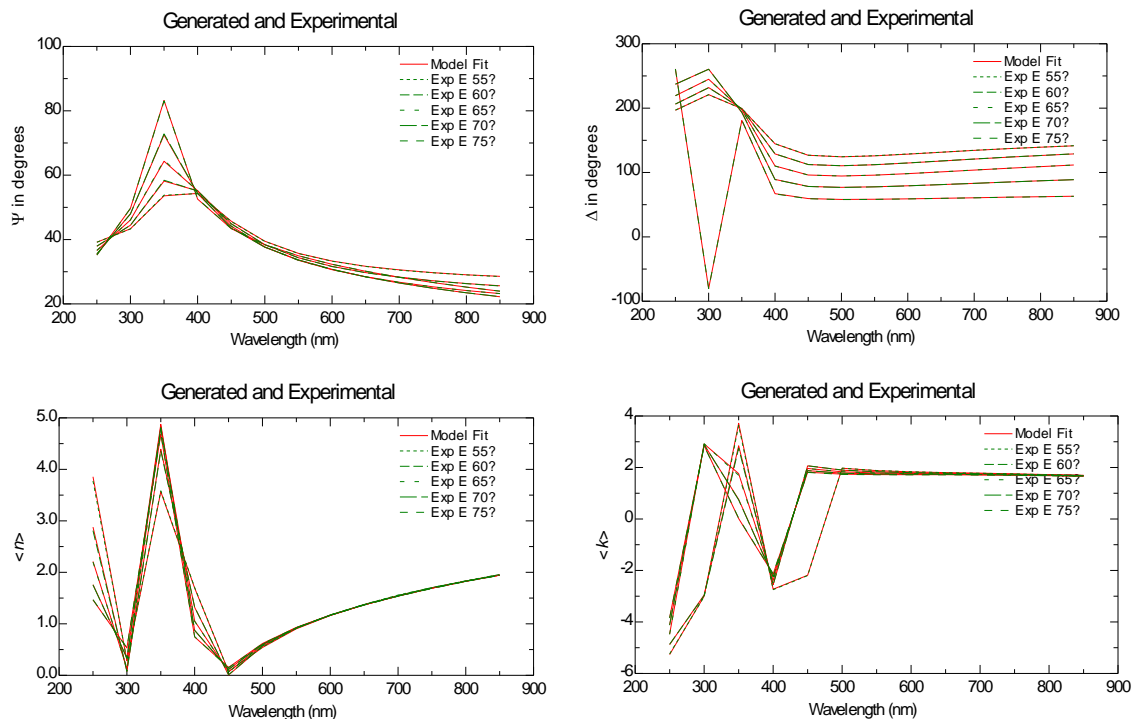
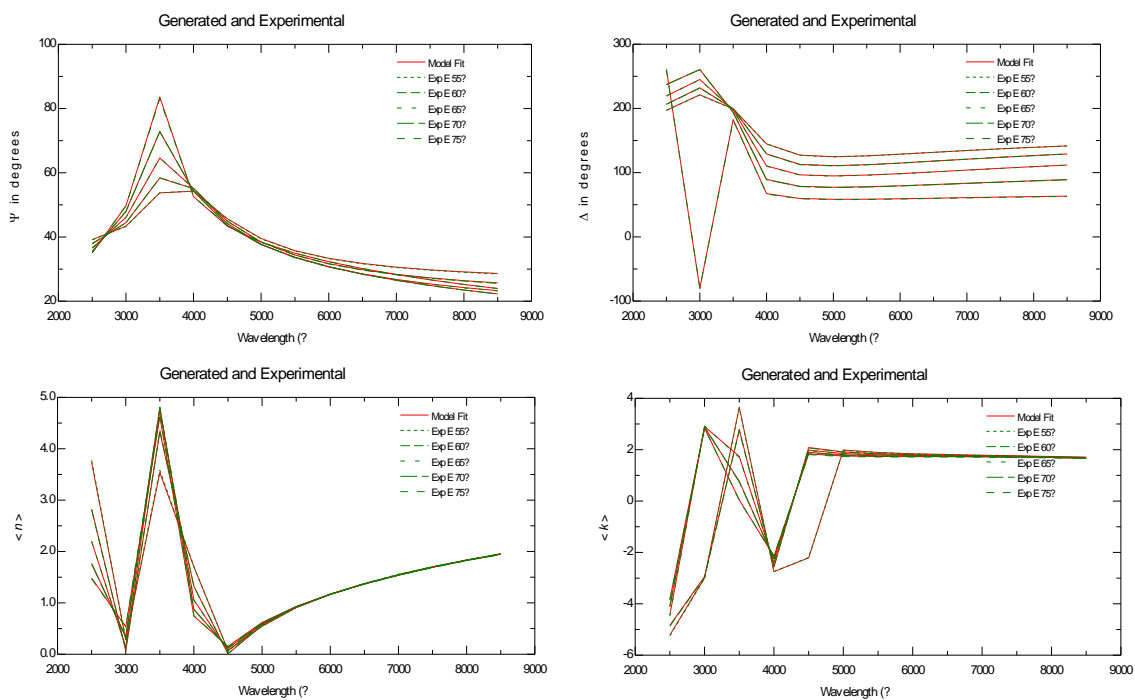


Figure S3. Ellipsometric fitting results using WVASE32 program (continued).

D-1) Al<sub>2</sub>O<sub>3</sub> bilayer layer from Al(NO<sub>3</sub>)<sub>3</sub>, fitting with EMA model



D-2) Al<sub>2</sub>O<sub>3</sub> bilayer layer from Al(NO<sub>3</sub>)<sub>3</sub>, fitting with simple model



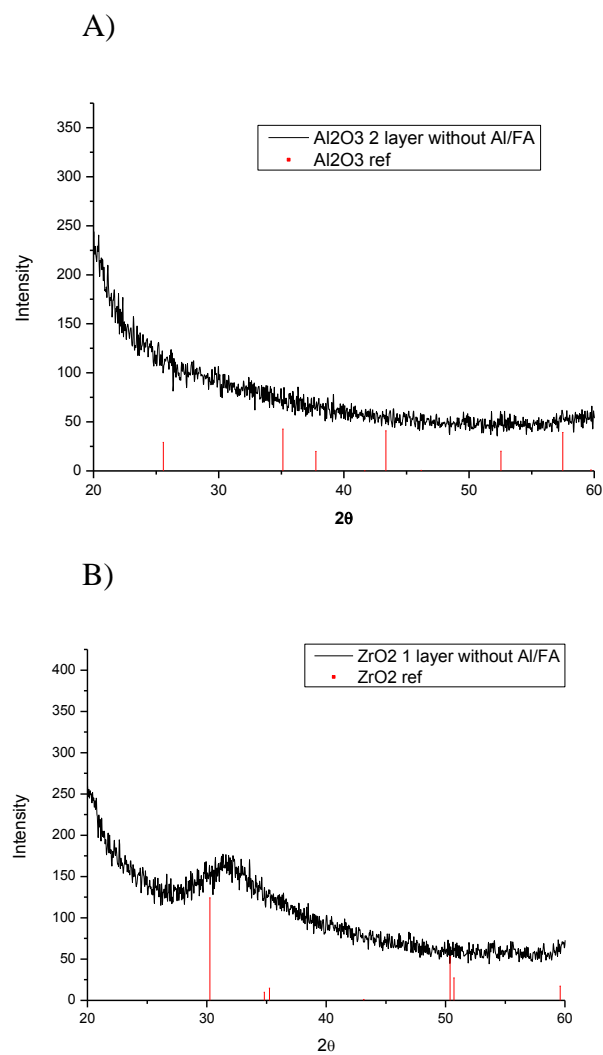


Figure S4. XRD results of (A) Al<sub>2</sub>O<sub>3</sub> and (B) ZrO<sub>2</sub> films on Si substrate.

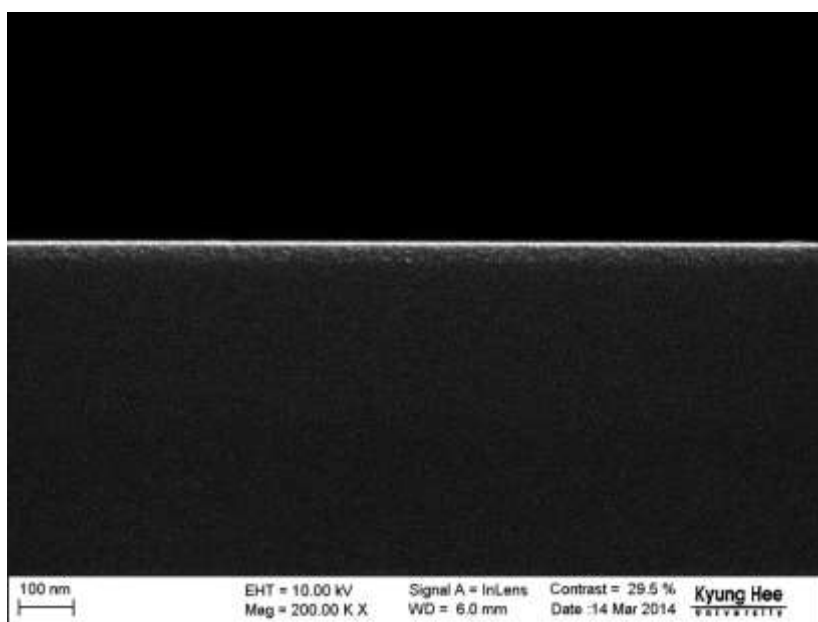


Figure S5. Contrast enhanced SEM image of Figure 3(B) to define the interface between  $\text{ZrO}_2$  layer and Si substrate.

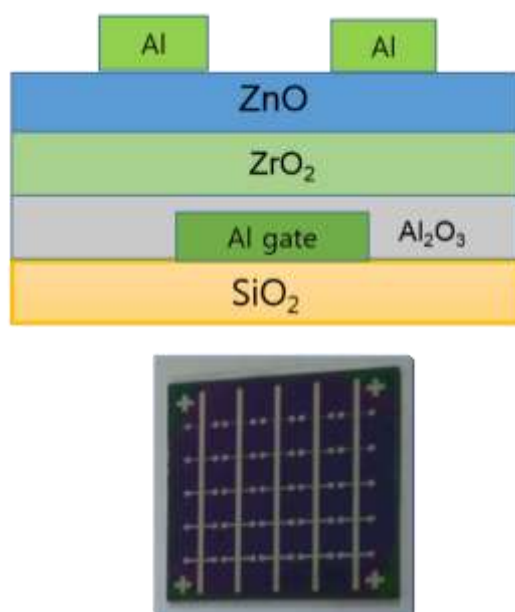


Figure S6. Schematic device structure and the photograph of ZnO TFT

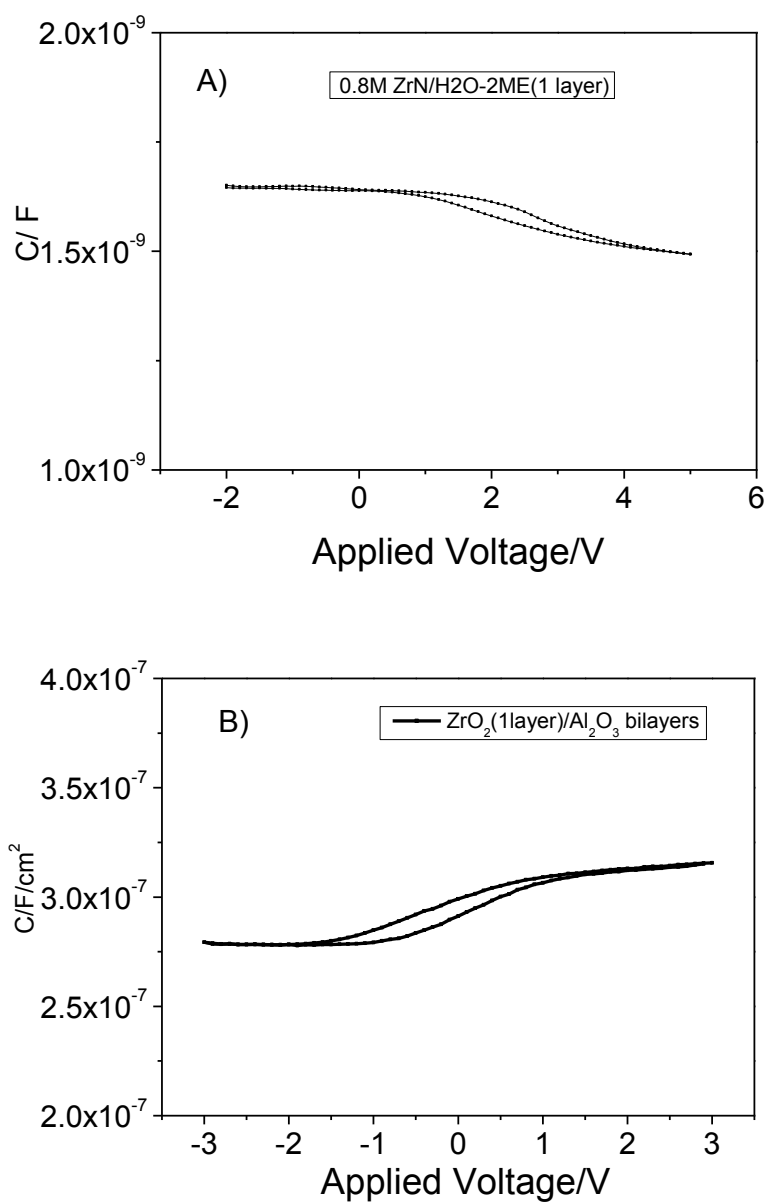


Figure S7. C-V characteristics of (a)  $ZrO_2$  MIS structure and (b) ZnO TFT device with  $ZrO_2/Al_2O_3$  bilayer at 100kHz. Hysteresis is evident in both scans.